On the flow of associative polymers past a sphere: Evaluation of negative wake criteria

A. J. Mendoza-Fuentes,[1] R. Montiel,[2] R. Zenit,[3] and O. Manero[3]
[1]*Facultad de Química, Universidad Nacional Autónoma de México, Apartado Postal 70-360, Mexico DF 04510, Mexico*
[2]*Universidad Autónoma Metropolitana Iztapalapa, Apartado Postal 55-534, Mexico DF 09340, Mexico*
[3]*Instituto de Investigaciones en Materiales, Universidad Nacional Autónoma de México, Apartado Postal 70-360, Mexico D.F. 04510, Mexico*

(Received 2 October 2008; accepted 9 February 2009; published online 18 March 2009)

A study on falling spheres descending in associative polymers with sphere-container ratios of 0.05–0.15 for various polymer concentrations and Weissenberg numbers is presented. The fluid exhibits constant viscosity over a wide range of small to moderate shear rates, and shear thinning for large shear rates. The simple shear rheology and linear viscoelasticity of these polymers are modeled with the BMP equation of state [F. Bautista, J. M. de Santos, J. E. Puig, and O. Manero, J. Non-Newtonian Fluid Mech. **80**, 93 (1999); O. Manero, F. Bautista, J. F. A. Soltero, and J. E. Puig, J. Non-Newtonian Fluid Mech. **106**, 1 (2002)], which enables the prediction of the extensional viscosity as a function of the strain rate. The particle image velocimetry technique allows the measurement of the velocity field in the rear of the sphere. The container wall affects the formation of the negative wake at a critical Weissenberg number, which closely corresponds to the region around the peak of extension thickening of the Trouton ratio in the solution. A characteristic strain rate is estimated from the distance of the sphere surface to the stagnant point where the velocity changes direction. Using these data, various criteria for the appearance of the negative wake are discussed. Conclusions reached by Dou and Phan-Thien [Rheol. Acta **43**, 203 (2004)] on the physical mechanisms for negative wake generation, are in agreement with the results exposed in this work. © *2009 American Institute of Physics*. [DOI: 10.1063/1.3090180]

I. INTRODUCTION

Sedimentation of spheres in complex fluids and associated phenomena such as the generation of negative wakes are still standing problems that require further examination to be properly understood. Rheological modifiers used in the paint and coating industry as well as in enhanced oil recovery processes usually involve a surface active polymer and suspending particles.[1] These polymers, namely, associative polymers, form an elastic network joined by electrostatic interactions and physical entanglements in the concentrated regime. The complexity of the flow behavior of falling spheres, in general and in particular, is manifested in interesting phenomena resulting from the viscoelastic, surface, and time-dependent properties of the fluid.[2] The study of these phenomena is the subject of the present investigation.

Within a historical perspective, Sigli and Coutenceau[3] performed flow visualization experiments with polyethylene oxide, a shear-thinning fluid. Results show the presence of a stagnant point located in the sphere wake. Past this point, there is a recirculation region where the fluid moves in the opposite direction to the sphere motion. As the sphere-container ratio is increased, the elastic effects are enhanced and also the magnitude of the negative wake for sphere-container ratios of 0.25 to 0.75. Hassager[4] found the same recirculation pattern in wakes generated by rising bubbles in polyacrylamide and glycerol viscoelastic solutions, and named this effect "negative wake." Thereafter, Bisgaard[5] reported that the magnitude of the negative wake is independent of the sphere-container ratio (within 0.04 and 0.18) in shear-thinning polyacrylamide-glycerol solutions.

Maalouf and Sigli[6] inferred that the necessary condition for negative wake generation in the flow past a sphere with various fluids and geometries was the shear-thinning properties and viscoelasticity of the fluid. Chilcott and Rallison[7] performed numerical simulations with a finite extensibility nonlinear elasticity (FENE) model with various values of the extensibility parameter (the FENE-CR model) aimed to predict the essential features of previous experiments. Lack of convergence for large values of the extensibility prevented the prediction of the negative wake. Nevertheless they concluded that the combination of extensibility and shear thinning are the main factors for negative wake generation. Further numerical simulations by Carew and Townsend,[8] Zheng *et al.*,[9] Harlen,[10] and Gervang *et al.*[11] did not predict the negative wake but an enlargement of the wake region as the model parameters were varied.

The first theoretical prediction of the negative wake was given by Jin *et al.*[12] using a shear-thinning Phan–Thien–Tanner fluid and thereafter by Zheng *et al.*,[13] suggesting that the presence of viscoelasticity and shear thinning are the main factors for negative wake generation. Most works try to describe qualitatively the causes that lead to negative wakes, although different fluids and sphere to container ratios make comparisons difficult. Bush[14] employed various shear-thinning polyacrylamide-glucose solutions maintaining the polymer concentration fixed but allowing various glucose

contents. An interesting trend was observed: as the glucose concentration decreases, the negative wake is detected, while the maximum in the velocity and position of the stagnant region move away from the sphere as the sphere-container ratio decreases. This behavior was attributed to the relation between the fluid elasticity and the magnitude of the extensional stresses in the wake region. Numerical simulations reveal that the negative wake appears when elasticity dominates, otherwise, the wake gets enlarged with no negative velocity. Consequently, as the ratio of the Weissenberg number to Trouton ratio (We/Tr) increases, negative wake generation is likely.

Using the FENE-CR model, Satrape and Crochet[15] predicted negative wakes in Boger fluids. The appearance of the wakes was related to the extensional properties of the model, particularly to the extensibility parameter. When this is small, negative wakes are predicted. These results agree with those of Harlen *et al.*[16] using the same model, including the displacement of the stagnant region farther away from the sphere as We increases.

In apparent disagreement are the works that sustain that negative wakes are the result of combined shear thinning and viscoelasticity[6,13] and those suggesting that their cause is the dominant contributions from the extensional properties of the fluid.[14,17,18] In the latter work[18] it is pointed out that these effects are produced by the existence of two opposing forces acting in the wake region behind the sphere. One of them is the relaxation of shear stresses generated in the equatorial region of the sphere that produce the flow reversal. This force is opposed to the extensional stresses generated in the wake region that produces an enlargement of the wake with the fluid moving in the same direction of the sphere. The parameter controlling the balance between these forces is the polymer extensibility, which limits the extensional viscosity of the polymer. Harlen *et al.*[18] made simulations with the FENE-CR, FENE-P, and Giesekus models, and found that in all cases, a reduction in the extensional stresses is predicted for small values of the extensibility parameter (or small Trouton ratios), that in turn are comparable with the magnitude of the shear stresses. In this situation, the negative wake is generated.

Arigo and Mckinley[19] suggested two criteria for the appearance of the negative wake in shear-thinning polyacrylamide solutions. These criteria point out that the ratio of the extensional stresses to shear stresses ($\tau_{\text{ext}}/\tau_{xy}$) is the important parameter and that the negative wake arises from the nonlinear response of the fluid at high Hencky strains.

Dou and Phan-Thien[20] found that, in general, the previous criteria are not always valid. Using the Maxwell, Oldroyd, Phan–Thien–Tanner (PTT), and FENE-CR fluid models, results show that the criterion N_1/τ_{ext} (N_1 is the first normal stress difference) is valid only when the velocity in the wake region is larger than the corresponding Newtonian value in both models. Furthermore, the criterion $\tau_{\text{ext}}/\tau_{xy}$ is applied only for fixed Deborah numbers. For PTT and FENE-CR models, it was demonstrated that it is the extensional property of the fluid that governs the appearance of negative wakes. Dou and Phan-Thien[20] found that the normal stress and the gradient of the normal stress are responsible for negative wake generation, while other factors could either strengthen or weaken the formation of the negative wake. This gradient of normal stress arises mainly from the balance within the shear stress and the pressure around the wake. The role of this shear stress gradient is to promote a negative normal stress gradient, leading to a shortening of the wake. In their analysis they found that the negative wake does not depend on streamline shifting, and that shear-thinning reduces the shear stress level and therefore weakens the formation of the negative wake, while the shear-thinning first normal stress coefficient enhances the velocity overshoot. Dou and Phan-Thien[20] proposed that a less strain-thickening extensional viscosity will promote the generation of a negative wake. The formation of a negative wake is then dependent on the relative magnitude of the gradient of the extensional viscosity with respect to extensional rate divided by the extensional viscosity. A small magnitude of this ratio will promote the formation of a negative wake. In a following paper, Dou and Phan-Thien[21] proposed a criterion for negative wake occurrence using the PTT, FENE-CR, FENE-P, and Giesekus models of a flow past a cylinder. In the case of the FENE-CR model, it is easier to generate a negative wake than with the FENE-P model, suggesting that the constant shear viscosity in the FENE-CR fluid enhances the velocity overshoot, and that the shear-thinning viscosity of the FENE-P fluid delays the negative wake generation. Moreover, Dou and Phan-Thien[21] proposed a method for calculating the value of the critical Weissenberg number based on the steady state value of the Trouton viscosity and reveals that wall proximity is not the governing mechanism for negative wake formation.

Thus, after reviewing various existing criteria for generation of negative wakes, it is easy to show that for all three, the extensional property of the fluid is the key factor for negative wake appearance. Notwithstanding, as pointed out by Arigo and McKinley,[19] the difference between the Bush and Harlen criteria is unimportant since for many polymeric fluids it is found experimentally that the first normal stress difference is directly related to the shear stress through a relationship which depends on the shear stress. Additionally, in the recent literature the role of elasticity, wall proximity, and shear-thinning effects in the generation of negative wake have not been clarified, and lack of experimental data testing the three criteria is a drawback. The present work aims to contribute to the understanding of the physical mechanism that governs the formation of negative wake by evaluating the various criteria proposed in the current literature.

This work undertakes an experimental study on the criteria for negative wake generation, using data of falling spheres in a container filled with an associative polymer [hydrophobic alkali soluble emulsion (HASE)] at various polymer concentrations in water. Particle image velocimetry (PIV) is used to measure the velocity field around the sphere, and by differentiation, the relevant strain rates are calculated. An average main extension rate is evaluated from the difference in velocities and distance from the sphere surface to the stagnant region where the flow reverses in an opposite direction to the sphere motion. A constitutive equation, the Bautista–Manero–Puig (BMP) model,[22,23] is used to predict

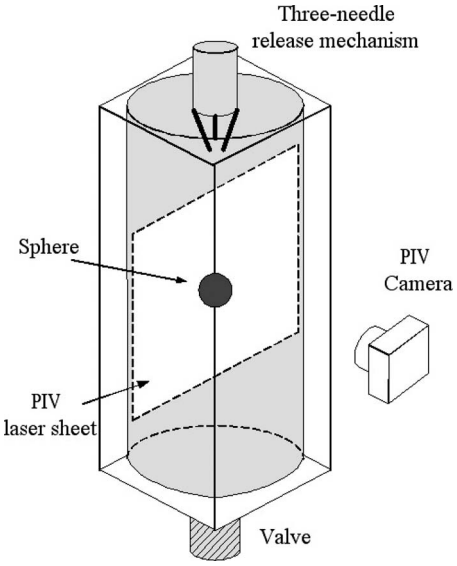

FIG. 1. Experimental apparatus.

the simple shear and extensional flow curves, and from these data, we obtain the parameters to evaluate the criteria for negative wake generation. Data not shown (but discussed) in this communication can be found in Mendoza-Fuentes.[24]

II. EXPERIMENTAL ARRANGEMENT

Experiments were performed in the device shown in Fig. 1. This device comprises a cylindrical container of 120 cm length and 12.7 cm diameter which has the test section and wherein the spheres descend. The container has a valve at the bottom to collect the spheres, which are released into the solution by a special mechanism to avoid surface and inertial effects. The cylindrical container is located inside a rectangular tank made of glass, with 150 cm height and 20.5 cm width filled with water. The similarity of the refraction indices of glass and water allows eliminating refraction effects of the curved cylinder-water interface.

Spheres were positioned below the free surface of the test fluid and left descend without rotation by a mechanical device made of three needles which place the spheres in the center of the container. To obtain a wide range of terminal velocities and sphere-container ratios, spheres of many sizes and densities were used. The physical properties of the spheres and the range of the experimental parameters attained with each type are shown in Table I.

For this problem, the two relevant dimensionless numbers are the Weissenberg number (We), Reynolds number (Re) defined as

$$\mathrm{We} = \lambda U/a, \tag{1}$$

$$\mathrm{Re} = aU\rho/\eta(\dot{\gamma}). \tag{2}$$

The characteristic shear rate of the flow is

$$\dot{\gamma} = U/a, \tag{3}$$

where ρ is the fluid density, a is the sphere radius, U is the terminal velocity, $\eta(\dot{\gamma})$ is the shear viscosity, and λ is the relaxation time which is the inverse of the crossing frequency of G′ and G″ [defined in Eqs. (9a) and (9b) below].

The flow field around descending spheres was obtained using a PIV system (from Dantec dynamics). Silver coated hollow glass spheres were used as tracer particles, which were added to the test liquid to obtain the PIV images as shown in Fig. 2(a). The FLOWMAP software (from Dantec) was used to determine the velocity fields. An example of the velocity fields is shown in Fig. 2(b). An adaptive cross correlation technique was used, with a final interrogation area of 32×32 pixels and an overlap of 50% in the horizontal direction and 75% in the vertical direction. Subsequently, a peak validation, moving average and special filter routines were applied. Additionally, the terminal velocity of the spheres was also measured from the PIV images. The position of the sphere was determined by the area devoid of tracers. By measuring the displacements of the sphere center in sequential images, the velocity was calculated with an uncertainty of 0.1%.

The HASE polymer (Acrysol TT-935 from Rohm and Haas) was dissolved in water at 1.0, 1.5, 2.0, and 2.5 wt %, adjusting the *p*H to 9–9.5 with a 2-amino-2-methyl-1-propanol 0.1*M* solution. It is well known that in this range of *p*H the polymer chain is very expanded and becomes water soluble, allowing the hydrophobic groups of the chain to associate to either groups of the same molecule or to groups of other molecules, hence forming intra- and intermolecular electrostatic associations, increasing the solution viscosity.[25]

TABLE I. Physical properties of the spheres used in this study.

Material	Density (g/cm^3)	Diameter (cm)	a/R	Re	We
Tungsten	14.95	0.635–1.27	0.05–0.1	0.01–1.01	0.41–3.53
Brass	8.57	0.635–1.9	0.05–0.15	0.002–0.86	0.16–2.0
Steel	7.98	0.635–1.9	0.05–0.15	0.002–0.75	0.15–1.8
Aluminum oxide	3.95	0.635–1.27	0.05–0.1	0.003–0.22	0.09–0.68
Aluminum	2.79	0.635–0.7874	0.05–0.062	4×10^{-4}–0.71	0.036–0.95
Teflon	2.30	0.635–1.9	0.05–0.15	0.003–0.74	0.05–0.73
Delrin	1.39	0.635–1.9	0.05–0.15	0.002–0.11	0.026–0.12
Nylon	1.14	0.635–1.9	0.05–0.15	0.02–0.12	0.03–0.12

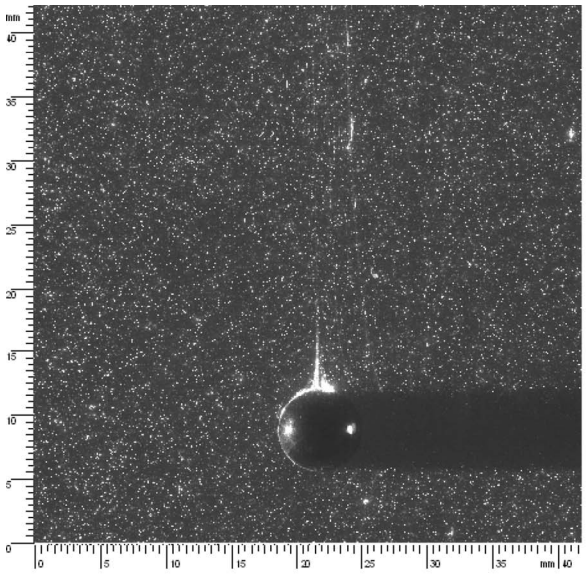

FIG. 2. (Color online) Typical PIV image (a) and its corresponding velocity field (b). The case shown corresponds to Re=0.418, We=1.95, and a/R =0.05. The scale to the left of the figure shows the length in millimeters. The unit length of the vectors (1 mm) corresponds to a velocity of 1 mm/s.

The solutions were left standing for 48 h previous to testing, and residual bubbles were extracted before the test.

A TA Instruments-AR 1000-N stress-controlled rheometer was used to measure the viscosity and first normal stress difference flow curves, in the shear rate range of $0.01-100\ s^{-1}$. Small amplitude oscillatory shear flow was used to obtain the variation of the loss (G'') and storage (G') modulus with frequency at 22 °C. Tests were performed with the cone and plate fixture, with 4 cm diameter and 1.59.14° cone angle.

III. MODELING AND FLUID RHEOLOGY

A rheological constitutive equation is used to obtain the model parameters to predict the simple shear and oscillatory data. From these parameters, the uniaxial extensional flow curve is then predicted and compared to available experimental data.

The equations of the rheological model considered here, namely, the BMP model,[22,23] are written in terms of the ith contribution to the stress according to

$$\underline{\underline{\tau}} = \sum_{i=1}^{n} \underline{\underline{\tau}}_i, \tag{4}$$

$$\underline{\underline{\tau}}_i + \lambda_i'(\underline{\underline{\tau}}_i, \underline{\underline{D}})\overset{\nabla}{\underline{\underline{\tau}}}_i = 2G_{0i}\lambda_i'(\underline{\underline{\tau}}_i, \underline{\underline{D}})\underline{\underline{D}}, \tag{5}$$

$$\lambda_i'(\underline{\underline{\tau}}_i, \underline{\underline{D}}) = \eta_i(\underline{\underline{\tau}}_i, \underline{\underline{D}})/G_{0i} = A_i^{-1}\lambda_{0i}, \tag{6}$$

$$\frac{dA_i}{dt} = \frac{1}{\lambda_i}(1 - A_i) + k_i(\lambda_{0i}/\lambda_{\infty i} - A_i)\underline{\tau}_i : \underline{D}, \tag{7}$$

where $\underline{\underline{\tau}}$ and $\underline{\underline{D}}$ are the stress and rate of deformation tensors, respectively; $\overset{\nabla}{\underline{\underline{\tau}}}$ denotes the upper-convected derivative of the stress tensor and λ', η, and G_0 stand for the variable relaxation time, the viscosity and the elastic shear modulus. A is a scalar and the three characteristic times $\lambda_0, \lambda_\infty, \lambda$ are the Maxwell relaxation time, the relaxation time at high frequencies and the structure relaxation time, respectively. Finally, k_i is the ith contribution to the destruction function.

For a single-mode model ($i=1$) Eq. (5) is the upper-convected Maxwell equation with variable relaxation time, which itself is a function of the scalar A that follows the evolution Eq. (7). The limits of A are one in creeping flows and λ_0/λ_∞ in strong flows. Equation (7) represents the changes in the structure due to the flow through a kinetic equation that follows the process of breakage and reformation of the structure. The first term on the right-hand side of Eq. (7) is identified with the reformation process, which is governed by the characteristic time λ. The second term is a function of the dissipation ($\underline{\tau} : \underline{D}$) and represents the breakage of the structure. When the ratio of the two time scales λ/λ_0 is much larger than one, the structure does not reform during the time scale of the external flow process and the system exhibits thixotropy. In steady state, the single-mode version of Eqs. (4)–(7) reduces to

$$\frac{1 + (\lambda k)(\lambda_0/\lambda_\infty)(\underline{\tau} : \underline{D})}{1 + \lambda k(\underline{\tau} : \underline{D})}\underline{\tau} + \lambda_0\overset{\nabla}{\underline{\tau}} = 2G_0\lambda_0\underline{D}, \tag{8}$$

where the time derivative contained in the upper convected derivative is equal to zero. In small deformation flows, Eq. (8) reduces to the linear Maxwell model. In small-amplitude oscillatory flow, the multimode version of Eq. (8) renders the well-known expressions of the storage and loss moduli.

$$G' = \sum_{i=1}^{n} G_{0i}\frac{\omega^2\lambda_{0i}^2}{1 + \omega^2\lambda_{0i}^2}, \tag{9a}$$

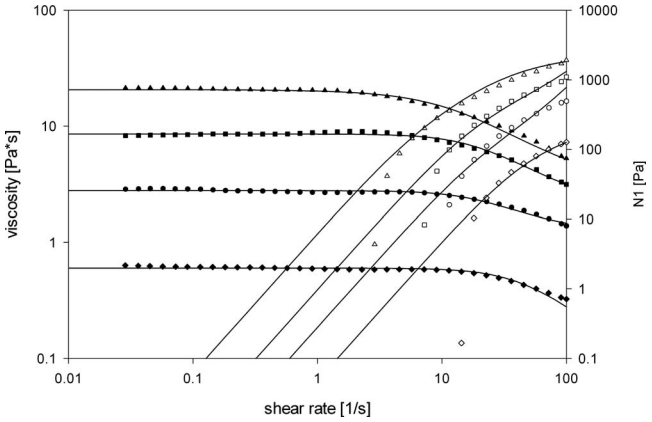

FIG. 3. Shear viscosity and first normal stress difference, solid and empty symbols respectively, for various polymer concentrations: (▲) 2.5%, (■) 2.0%, (●) 1.5%, and (♦) 1.0%. Experimental data are compared to predictions of the model considered here (solid lines).

$$G'' = \sum_{i=1}^{n} G_{0i} \frac{\omega \lambda_{0i}}{1 + \omega^2 \lambda_{0i}^2}, \tag{9b}$$

provided that the zero strain-rate viscosity is

$$\eta_0 = \sum_{i=1}^{n} G_i \lambda_i. \tag{10}$$

In steady simple shear flow the model predicts, for a single mode, the following expressions for the fluidity and first normal stress difference:

$$\varphi_{ss} = \tfrac{1}{2}[-(k\lambda\dot{\gamma}^2 - \varphi_0) + ((k\lambda\dot{\gamma}^2 - \varphi_0)^2 + 4k\lambda\dot{\gamma}^2\varphi_\infty)^{1/2}] \tag{11}$$

and

$$N_1 = \frac{2\dot{\gamma}\tau}{G_0\varphi_{ss}}. \tag{12}$$

For steady extensional flow, we use the modification of the model as suggested by Boek *et al.*,[26] namely,

$$(\phi - \phi_0)(G_0\phi - 2\dot{\varepsilon})(G_0\phi + \dot{\varepsilon}) = 3\lambda\left(\frac{k}{\eta_\infty}\right)G_0^2\phi\dot{\varepsilon}^2, \tag{13}$$

$$N_1 = \frac{\phi - \phi_0}{\lambda(k/\eta_\infty)\dot{\varepsilon}} + \eta_S\dot{\varepsilon}, \tag{14}$$

where N_1 and $\dot{\varepsilon}$ are the extensional stress and extension rate, respectively. In addition, $\phi = 1/\eta_P$ is the polymer fluidity, $\phi_0 = 1/\eta_0$ and $\eta_e = (N_1/\dot{\varepsilon})$ is the extensional viscosity.

IV. RESULTS

A. Simple shear and uniaxial extensional flow

In Fig. 3, the shear viscosity and first normal stress difference under simple shear are plotted with shear rate. Data and predictions are shown for four polymer concentrations. At low shear rates the first Newtonian region, where the viscosity is constant, spans over various decades of shear rates. For moderate shear rates, shear thinning is apparent.

From 0.01 to 2 s^{-1}, the first Newtonian plateau is observed for the more concentrated solutions, while for the less concentrated this plateau extends to shear rates around 10 s^{-1}.

In the intermediate regime a region of slight shear thickening is observed (2 wt %). At high shear rates, the onset for shear thinning occurs at lower shear rates as the concentration increases. Notice the large span of constant viscosity for the more diluted system, similar to Boger fluids.

The first normal stress difference increases with concentration and shows the Maxwellian quadratic dependence with shear rate at low shear rates and a departure for larger shear rates. The departure from the quadratic dependence is attained at lower shear rates for the more concentrated solution. An excellent agreement of the model predictions with experimental data is observed. In Table II, model parameters for each concentration are shown, requiring a single mode. The solution with the highest concentration requires two modes for an adequate prediction.

Figure 4 shows the linear viscoelastic data and model predictions in the frequency range from 0.1 to 100 rad/s for the four concentrations considered here. The crossing frequency diminishes with polymer content, implying an increasing average relaxation time with concentration. The magnitude of the plateau modulus also increases with concentration, thus exhibiting a more entangled network as the polymer content increases. Most data are fitted with five relaxation modes and the fitting parameters are shown in Table III. Comparing the number of modes in simple shear to those in the linear viscoelastic regime, it is apparent that under

TABLE II. Model parameters under simple shear flow.

Concentration (wt %)	ϕ_0	ϕ_∞	k	λ	G_0
1.0	1.666	90	0.0002	0.040	13
1.5	0.360	0.77	0.0050	0.050	55
2.0	0.117	0.45	0.0008	0.060	150
2.5	0.047	0.25	0.0003	0.060	220
	0.001	0.04	0.0600	0.001	500

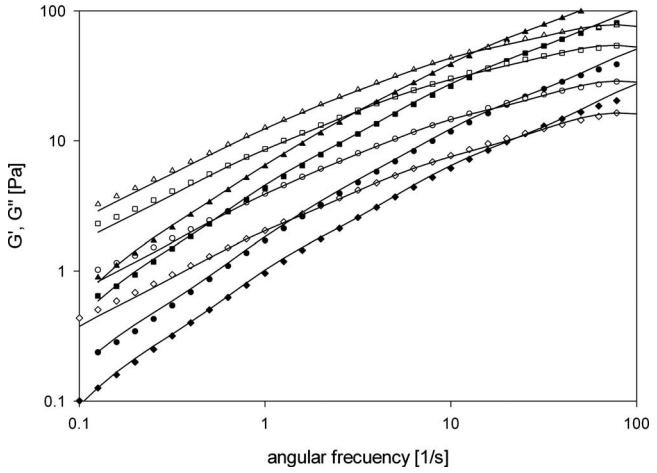

FIG. 4. Storage and loss modulus, solid and empty symbols, respectively: (▲) 2.5%, (■) 2.0%, (●) 1.5%, and (♦) 1.0%.

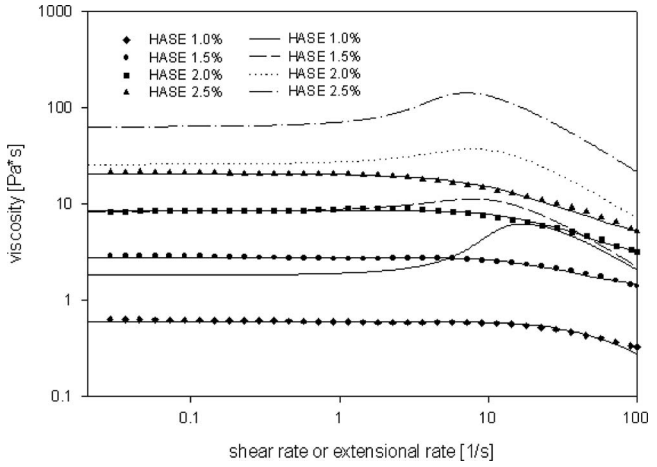

FIG. 5. Shear viscosity (symbols) and model predictions for shear and uniaxial extensional flows (lines).

simple shear the structure is in some form modified and the relaxation time spectrum is reduced to mostly one dominant average relaxation time due to the flow.

In Fig. 5, model predictions for uniaxial extensional flow and simple shear data are shown for the four concentrations. A region of constant extensional viscosity at low extension rates ($\dot{\varepsilon} < 10$) is followed by a strain-thickening region. The onset for the increasing viscosity coincides with that of shear thinning, and the magnitude of the maximum in the extensional viscosity increases with concentration, although this increase is more pronounced in the dilute system with respect to the zero strain-rate viscosity. Once again, as in simple shear, the onset for strain thickening shifts to lower strain rates as concentration increases. This behavior has been associated with the evolution of intramolecular junctions into intermolecular links as flow strength increases. The formation of an intermolecular network results in increasing elasticity and hence strain thickening. Because extensional flow deforms the system more drastically than simple shear, the extension thickening is normally more pronounced than shear thickening. At larger strain rates, the intermolecular associations break, leading to structure rupture and hence strain thinning.

To validate the extensional flow predictions, model results are compared to available experimental data of the HASE polymer. In Fig. 6, data from Tan *et al.*[27] (symbols) and model predictions (lines) of the extensional viscosity versus extension rate are depicted. A very good agreement is displayed for three polymer concentrations.

B. Flow past a sphere

Since we were able to vary the value of the aspect ratio a/R, Re, and We numbers independently for each liquid, it was possible to evaluate their individual effects in the formation of the negative wake. In the following figures, the velocity profiles along the central streamline past the sphere, normalized with the sphere velocity, are depicted. The maximum velocity is the sphere velocity ($U/U_s = 1$) and the minimum corresponds to the stagnant fluid at the rear of the sphere ($U/U_s = 0$), where the fluid reverses direction and induces the negative wake.

1. Weissenberg number effect for a fixed a/R

In Figs. 7(a) and 7(b) the normalized sphere velocity is plotted with the nondimensional distance from the sphere for a fixed aspect ratio of 0.05 and for two concentrations (1.0 and 1.5 wt %). The velocity in Fig. 7(a) decreases as We increases and no negative wake is observed for We number lower than 1.0. For $We > 1.0$, a slight negative value is depicted far downstream the sphere ($z/a \approx 33$). In Fig. 7(b) the concentration is 1.5 wt % for the same aspect ratio ($a/R = 0.05$) and for three We numbers. The negative wake is ap-

TABLE III. Model parameters in small-amplitude oscillatory shear flow.

C (wt %)	1.0		1.5		2.0		2.5	
	G_0	λ_i	G_0	λ_i	G_0	λ_i	G_0	λ_i
Mode 1	30.79	0.011	53.39	0.01	96.52	0.01	140.4	0.011
Mode 2	4.02	0.069	15.33	0.08	23.46	0.05	48.3	0.077
Mode 3	4.38	0.151	3.43	0.38	17.46	0.16	13.6	0.355
Mode 4	1.45	0.905	1.55	1.13	1.14	0.53	5.04	1.183
Mode 5	0.24	6.875	0.41	7.66	5.30	0.98	1.8	6.188
Mode 6					1.17	6.79		

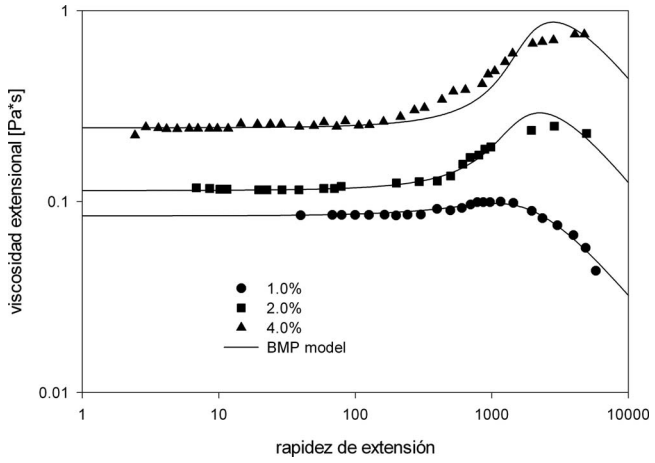

FIG. 6. Experimental data [from Tan *et al.* (Ref. 27)] of the extensional viscosity vs extension rate (symbols) and model predictions (lines).

parent, comprising the negative velocities with depths increasing with We number. The position of the stagnant point where the flow reverses shifts closer to the sphere as We increases, while the wake amplitude also increases with We. The position of the stagnant point is $12 \leq z_{stag}/a \leq 18.5$. Meanwhile, the length of the negative wake extends to more

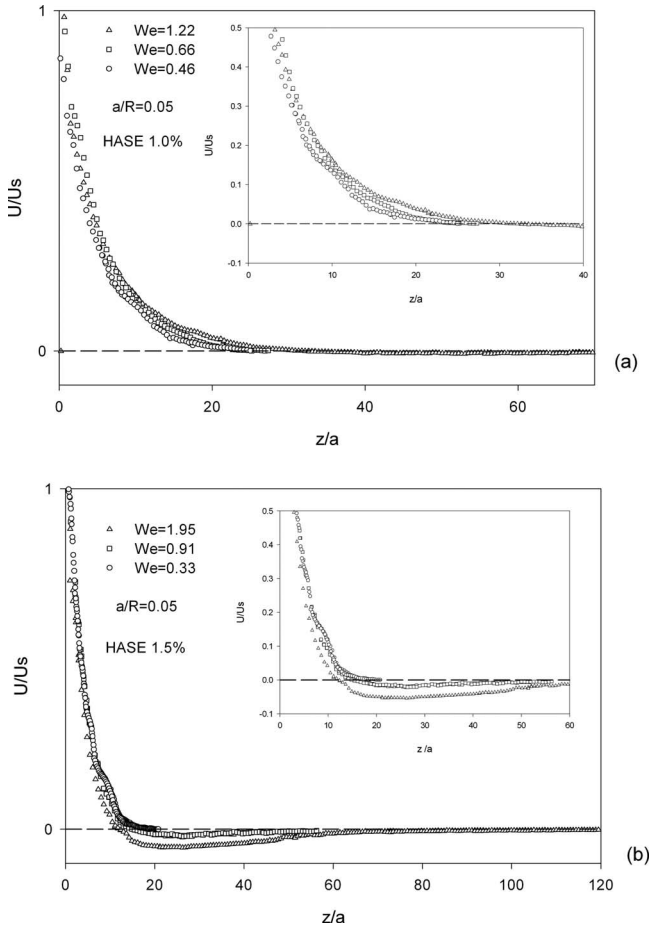

FIG. 7. Normalized velocity vs distance from the sphere for various We numbers. (a) 1.0 wt %, $a/R=0.05$, $0.2 \leq Re \leq 0.61$, (b) 1.5 wt %, $a/R=0.05$, $0.02 \leq Re \leq 0.2$.

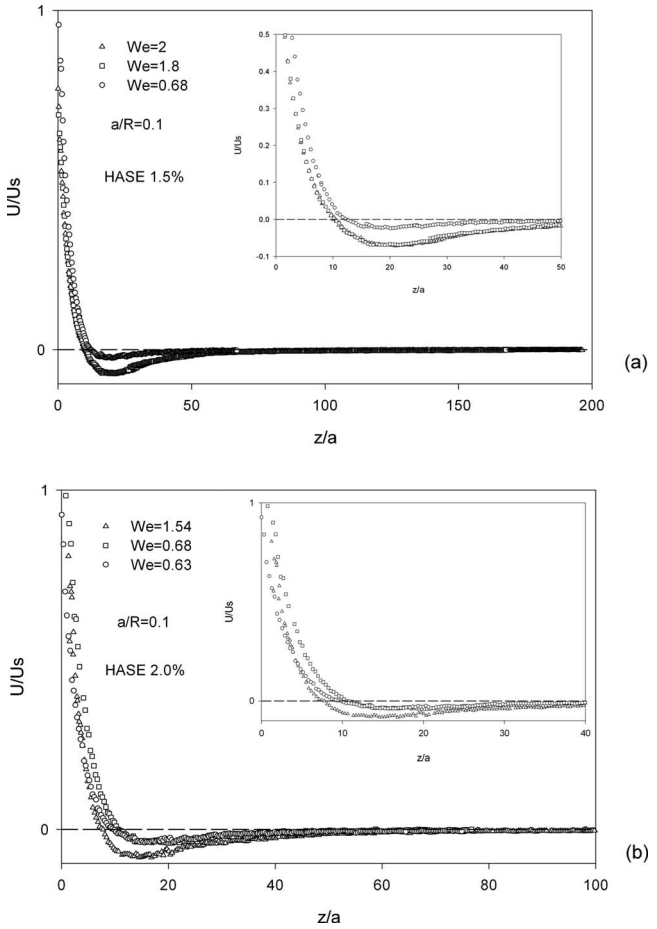

FIG. 8. Normalized velocity vs distance from the sphere for various We numbers. (a) 1.5 wt %, $a/R=0.1$, $0.22 \leq Re \leq 0.86$, (b) 2.0 wt %, $a/R=0.1$, $0.05 \leq Re \leq 0.17$.

than 120 times the sphere radius. Results in Figs. 7(a) and 7(b) show that for these cases the negative wake appears for We numbers around 1.0.

For a larger aspect ratio ($a/R=0.1$), in Figs. 8(a) and 8(b) the minima of the negative wakes is more pronounced as We increases. In this case, negative wakes are formed for We numbers lower than 1.0. Indeed, these appear for $We > 0.6$. and $We > 0.36$ for the 1.5 and 2.0 wt % polymer concentrations, respectively. The position of the stagnant region is $8 \leq (z_{stag}/a) \leq 12$. For larger concentrations, the position of the stagnant point and wake amplitude follow the same trends observed before. Lastly, for the largest concentration (2.5 wt %), the negative wake appears at We numbers as low as 0.3 (not shown).

Dou and Phan-Thien[21] considered the steady state value of the Trouton ratio to locate the critical We number corresponding to the negative wake apparition. Their analysis of the experimental data reveals that a less strain-hardening extensional viscosity will promote the generation of a negative wake. In our analysis, the critical We is found corresponding closely to the region around the peak of Trouton ratio (Fig. 9) and at the onset of extension thinning. As will be shown later in Sec. III, the critical values obtained with the BMP model for each system agree well with the critical values obtained experimentally. The critical We numbers for the ap-

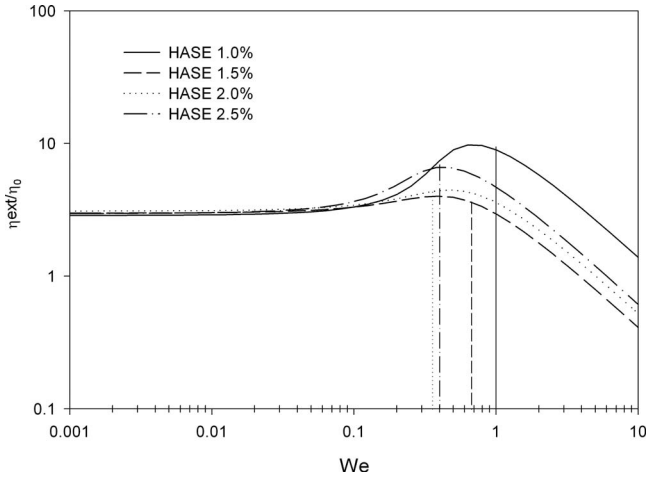

FIG. 9. Trouton ratio as a function of Weissenberg number. Vertical lines indicate the critical We number for negative wake appearance.

pearance of the negative wake are plotted in Fig. 9. A trend is observed in that they are smaller as the concentration increases.

2. Effect of the sphere-container ratio for a fixed We

Figures 10(a) and 10(b) illustrate the effect of the aspect ratio (sphere container) for two polymer concentrations, maintaining We nearly constant. The overall effect of the aspect ratio is to increase the magnitude of the minima in the velocity, shifting the stagnant point closer to the sphere. The stagnant point position is located at $9 \leq z_{stag}/a \leq 12$ and $8 \leq z_{stag}/a \leq 12$ for the 1.5 and 2.5 wt % polymer concentrations, respectively. As the solution viscosity increases, the extension of the wake is reduced considerably.

3. Inertial effects

The Reynolds number is varied for two aspect ratios (not shown). The overall effect of inertia is to shift the stagnant point farther away from the sphere. Slight fluctuations in the velocity are detected for large values of Re (Re > 1).

C. Polymer concentration effects

1. Fixed aspect ratio

Varying polymer content does not influence the position of the stagnant point and the curves almost superimpose from the sphere to the stagnant point. Past the stagnant region, it is apparent that the magnitude of the minima is larger for the more diluted systems, and in the most concentrated system the negative wake disappears. Upon increasing the wall effect same results are obtained, but the magnitude of the minima increases (figures not shown).

2. Fixed Weissenberg number

In this case, the wall proximity has a large effect on the negative wake characteristics. As the aspect ratio increases, the stagnant point shifts closer to the sphere and the magnitude of the minima increases (not shown). The more diluted

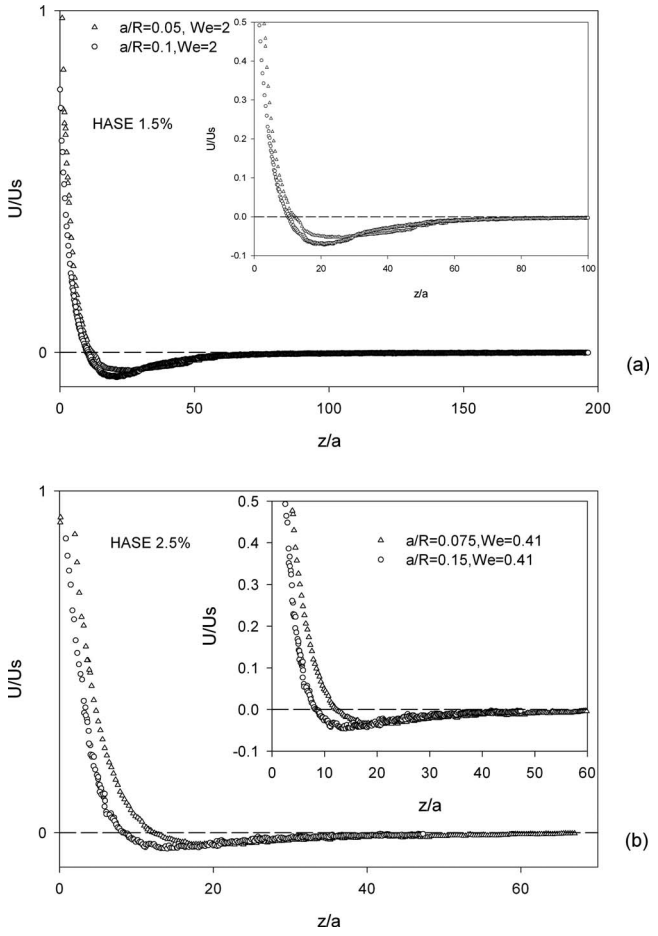

FIG. 10. Wall proximity effect on the negative wake generation. (a) 1.5 wt %, $0.2 \leq Re \leq 0.86$; (b) 2.5 wt %, $0.009 \leq Re \leq 0.03$.

solution generates smaller magnitudes, since the critical We number is barely attained and is larger in this case than in more concentrated systems (see Fig. 9).

For the combined fixed We number and fixed aspect ratio (Fig. 11), it is clear that increasing concentration produce a stronger flow reversal and the stagnant point shifts closer to the sphere in the range $9.5 \leq z_{stag}/a \leq 12$. Notwithstanding, although wall proximity increases the strength of the negative wake, it is not the dominant mechanism for its generation. Solution viscosity also contributes largely to the negative wake characteristics. In fact, the negative velocity is larger in the 2 wt % solution than in the 2.5 wt % solution. This effect was discussed by Dou and Phan-Thien,[20] and it is likely to be rather related to the extensional deformation of the liquid.

D. Summary of experimental results

The overall results described previously are in agreement to those of Sigli and Coutanceau,[3] in that the negative wake, for both We and a/R, is enhanced with increasing both parameters simultaneously to shifting the stagnant point closer to the sphere. Nevertheless, the positions of the stagnant points found in our work are extended farther away than those found by Sigli and Coutanceau. The position of the stagnation point in Sigli and Coutanceau data is 2.5

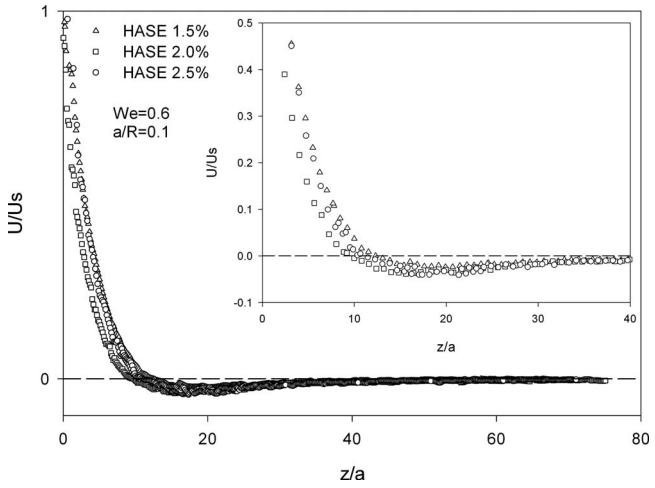

FIG. 11. Effect of concentration maintaining the aspect ratio and We number constant.

TABLE IV. Criteria for negative wake generation.

Author	Criteria	Negative wake
Bush[a]	$\frac{We}{Tr} \approx \frac{N_1}{\Delta\tau_{ext}}$	Large values
Harlen[b]	$\frac{\Delta\tau_{ext}}{\tau_{xy}}$	Small values
Arigo and McKinley[c]	$\frac{N_1}{\Delta\tau_{ext}}$	Large values
	$\frac{\Delta\tau_{ext}}{\tau_{xy}}$	Small values
Dou and Phan-Thien[d]	$(\partial\eta_{ext}(\dot{\varepsilon})/\partial\dot{\varepsilon})/\eta_{ext}(\dot{\varepsilon}) - \frac{1}{\dot{\varepsilon}}$	Small values

[a]Reference 14.
[b]Reference 18.
[c]Reference 19.
[d]References 20 and 21.

$\leq z_{stag}/a \leq 3.1$ for aspect ratios of $a/R < 0.4$ and for aspect ratios of $0.5 \leq a/R \leq 0.75$, a larger effect of the aspect ratio on the position of the stagnant point is found, i.e., $1.8 \leq z_{stag}/a \leq 2.4$.

Likewise, these tendencies have been validated theoretically with the Phan-Thien–Tanner and FENE-CR models by Dou and Phan-Thien.[20] Data of this work and that of Sigli and Coutanceau agree with predictions of negative wakes generated by Dou and Phan-Thien. Moreover, the critical value of Weissenberg numbers found in this work ($We > 0.6$ and $We > 1.0$) agree with those found by simulations using the above models in fluids with different extensional properties. Furthermore, data and simulations suggest that the negative wake may occur in solutions with low polymer concentrations without wall effects.

V. EVALUATION OF DIFFERENT NEGATIVE WAKE CRITERIA

As shown in Table IV, various criteria for negative wake generation have been proposed in the current literature. In the first two criteria, Bush[14] and Harlen[18] proposed that the negative wake appears when the magnitude of the extensional stresses is small compared to the magnitude of the shear stresses. Arigo and Mckinley[19] suggested a modification of the previous criteria allowing the first normal stress difference under shear to be included. However, it is not readily apparent which of the two expressions gives the necessary ingredients for negative wake generation. After comparison of their experimental data to those of Sigli and Coutanceau[3] and Bisgaard *et al.*,[5] Arigo and McKinley[19] proposed that the negative wake formation depends strongly on the nonlinear rheological properties of the solution.

According to Dou and Phan-Thien,[20] the criterion by Bush[14] is only valid when an upstream shift of the streamlines around the sphere appears, and fails when a downstream shift is observed. Furthermore, in the Harlen[18] criterion, comparison can be made only at constant We, and fails for large We. Dou and Phan-Thien[20] suggested that the negative wake formation is closely linked to the magnitude of the gradient of the extensional viscosity with respect to the extension rate divided by the value of the extensional viscosity. A low value of this relation means that a less strain-thickening extensional viscosity will promote negative wake appearance. Later, by analyzing the behavior of the axial velocity in the wake of the sphere, Dou and Phan-Thien[21] established the critical condition of negative wake generation: when the relation mentioned above tends to be equal to the reciprocal of the extension rate (see Table IV).

In most works so far, the characteristic extension rate is defined as $\dot{\varepsilon} = (\dot{\gamma}/\sqrt{3})$. However, to associate characteristic kinematics to the wake behind the sphere, the extension rate may be measured there, since along the centerline in the rear of the sphere the shear rate is zero (as in uniaxial extension). A characteristic average extension rate is proposed here consisting in the sphere velocity divided by the distance (d) from the back of the sphere to the stagnation point where the velocity of the flow is zero, namely, $\dot{\varepsilon} = (U/d)$. Together with the definition of the characteristic shear rate $\dot{\gamma} = (U/a)$, the first normal stress difference and the shear stress can be evaluated at the characteristic shear rate, using Fig. 2 to determine N_1 and τ_{xy}. The extensional viscosity, in turn, can be determined at a given extension rate $\dot{\varepsilon}$ using Fig. 4, and hence the extensional stress $(\Delta\tau_{ext})$ is given by $\Delta\tau_{ext} = (\tau_{zz} - \tau_{rr}) = \eta_{ext}(\dot{\varepsilon})\dot{\varepsilon}$. For Dou and Phan-Thien's criterion, the gradient of the extensional viscosity is evaluated by differentiation of the point of maximum velocity of the fluid (sphere velocity) $(U/U_s = 1)$ and the point of null velocity (stagnation point where the flow reverses) $(U/U_s = 0)$. Finally, the We number is calculated according to Eq. (1).

In Figs. 12–15, the criteria for negative wake generation proposed in the current literature are exposed. For each solution in Figs. 12(a)–12(c), 13(a)–13(c), 14(a)–14(c), and 15(a) the criterion suggested by Dou and Phan-Thien is shown. For low polymer concentrations (1 and 1.5 wt %) a well-defined limit for wake formation is shown, namely, that the negative wake forms when $(\partial\eta_{ext}(\dot{\varepsilon})/\partial\dot{\varepsilon}/\eta_{ext}(\dot{\varepsilon})) - (1/\dot{\varepsilon})$ is near zero. A critical We number is also determined, such as for $We \geq 1$, the negative wake is generated. Notwithstanding, upon increasing polymer concentration (2 and 2.5 wt %) a

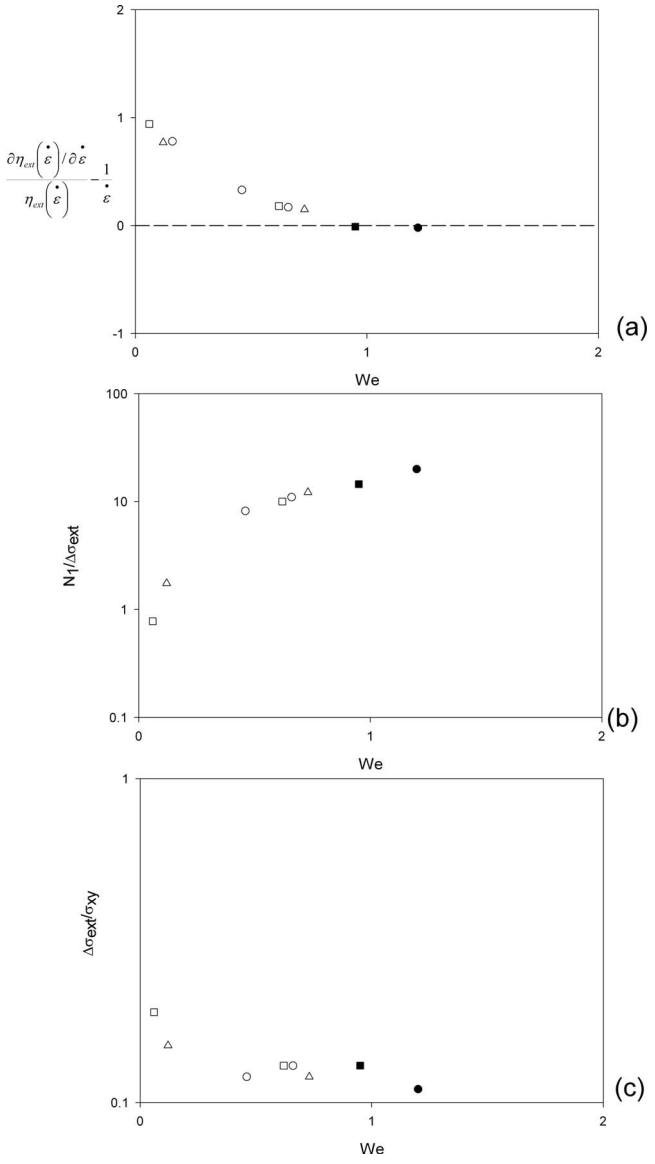

FIG. 12. Evaluation of criteria for negative wake generation (1.0 wt %). (a) Dou and Phan-Thien criterion, (b) Bush criterion, and (c) Harlen criterion. The symbols in black represent negative wake apparition, a/R=0.05 (circles), a/R=0.0625 (squares), and a/R=0.075 (triangles).

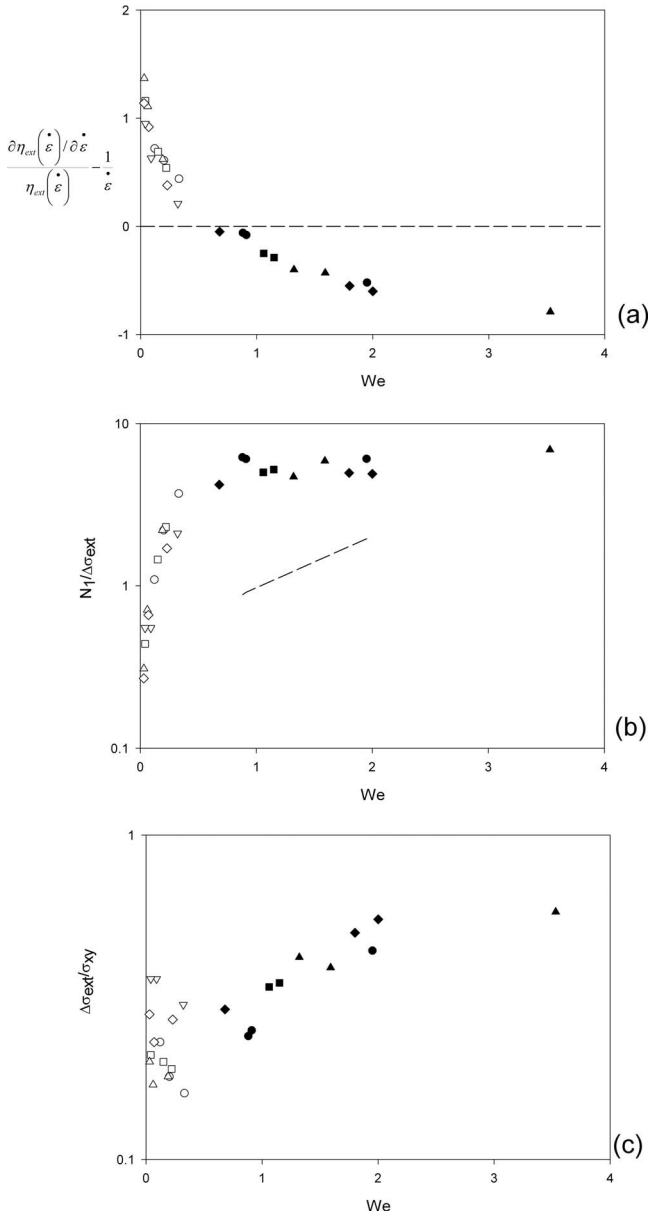

FIG. 13. Evaluation of criteria for negative wake generation (1.5 wt %), (a) Dou and Phan-Thien criterion, (b) Bush criterion, and (c) Harlen criterion. The symbols in black represent negative wake apparition, a/R=0.05 (circles), a/R=0.0625 (squares), a/R=0.075 (triangles), a/R=0.1 (diamonds), and a/R=0.15 (inverse triangles).

decrease in the critical We number is observed in accordance to Fig. 9. Following Dou and Phan-Thien, a less strain-hardening extensional viscosity will promote the generation of a negative wake, such that if the thickening is weak, formation of negative wakes is promoted. The critical We number is reduced as concentration increases, since the onset for extension thinning is shifted to lower extension rates, as observed in Fig. 9. Therefore, a close relation between the critical We around the peak and at the onset for extension thinning and that shown in Figs. 12(a)–12(c), 13(a)–13(c), 14(a)–14(c), and 15(a) for negative wake generation is apparent. For these higher polymer concentrations, the points between dashed lines indicate the presence of a negative wake situated around the peak of the Trouton ratio. In the case of the 2.0 wt % solution, the dashed lines show the presence of a weak negative wake, and as We increases, the negative wake is enhanced. For the 2.5 wt % solution, the effect of the container wall is strong [Fig. 10(b)] which accentuates the strength of the wake (the level of extensional deformation increases).

The amplitude of the wake increases with extension rate, in agreement to previous results of Secs. IIA–IIC. These tendencies are independent of the sphere-container ratio, evidencing that the main mechanism for wake generation does not depend strongly on the aspect ratio. This effect only accentuates the wake formation in concentrated solutions, where viscosity effects are important.

According to the Bush criterion [see Figs. 12(b), 12(c), 13(a)–13(c), 14(a)–14(c), 15(a), and 15(b)] in the low concentration regime the negative wake appears when We=1, while in the more concentrated systems, this appears at lower

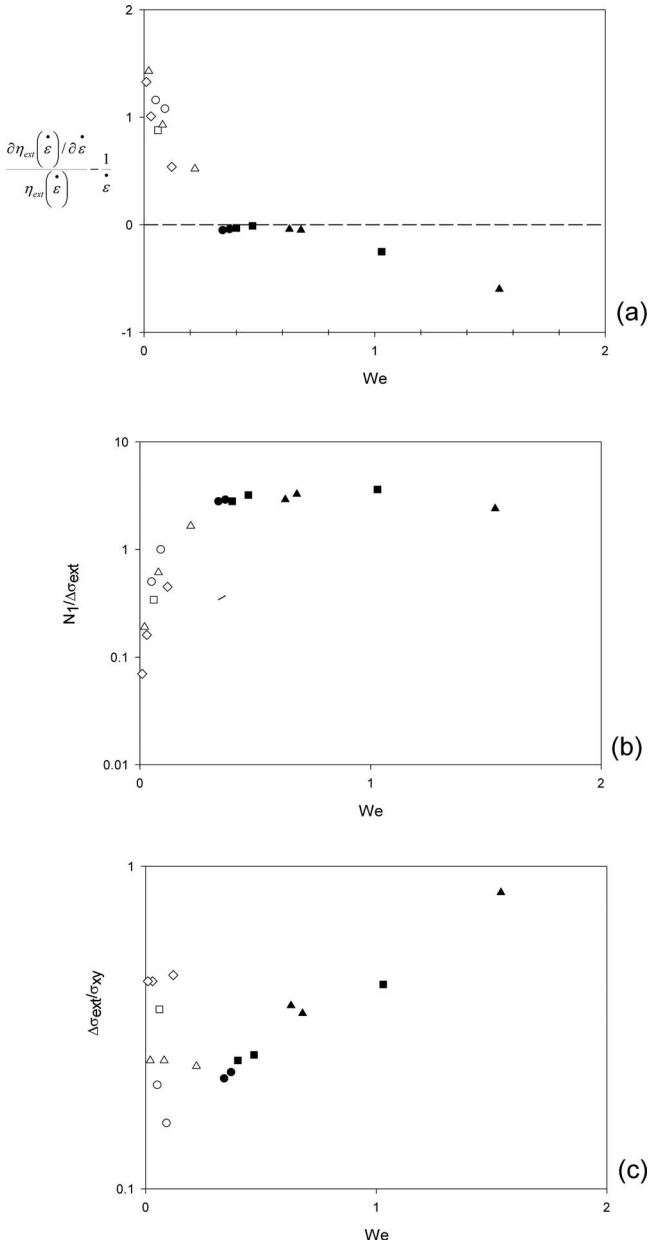

FIG. 14. Evaluation of criteria for negative wake generation (2.0 wt %), (a) Dou and Phan-Thien criterion, (b) Bush criterion, and (c) Harlen criterion. The symbols in black represent negative wake apparition, a/R=0.0625 (circles), a/R=0.075 (squares), a/R=0.1 (triangles), and a/R=0.15 (diamonds).

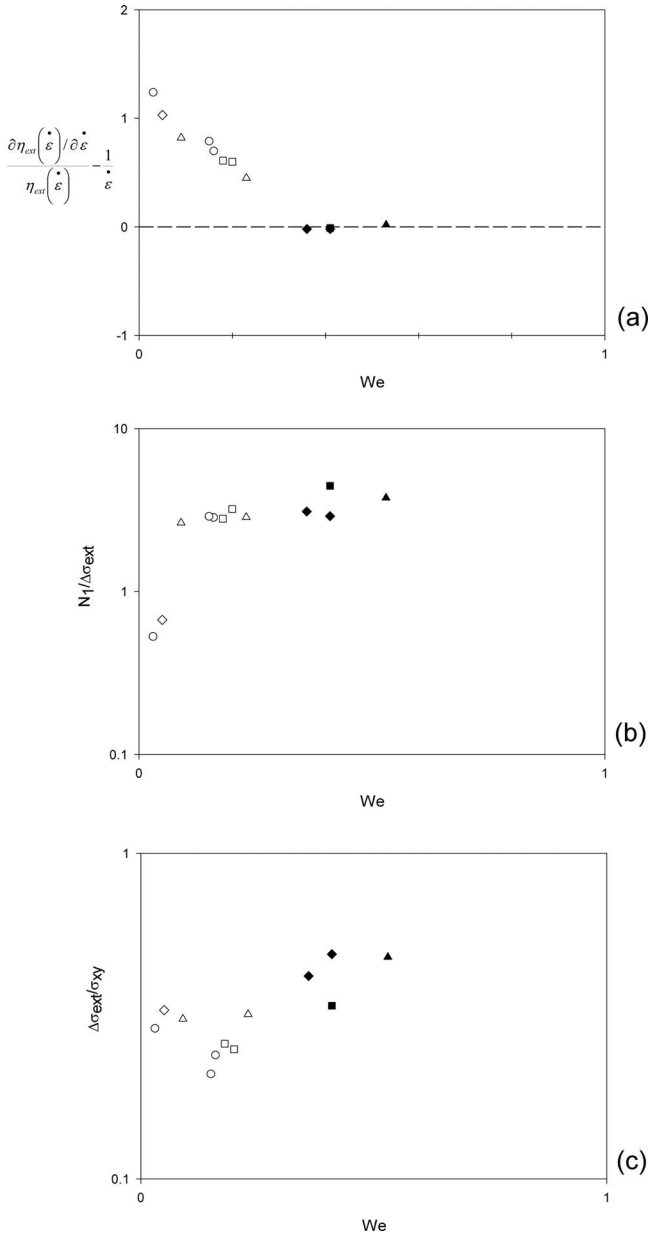

FIG. 15. Evaluation of criteria for negative wake generation (2.5 wt %), (a) Dou and Phan-Thien criterion, (b) Bush criterion, and (c) Harlen criterion. The symbols in black represent negative wake apparition, a/R=0.0625 (circles), a/R=0.075 (squares), a/R=0.15 (triangles), and a/R=0.15 (diamonds).

We numbers. This result derives from same argumentation exposed for Fig. 9, related to the onset for extension thinning. For larger We numbers (We>1) the ratio becomes We independent, effectively demonstrating the importance of the extensional properties of the solution in the negative wake formation.

Harlen's criterion,[18] shown in Figs. 12(c), 13(a)–13(c), 14(a)–14(c), and 15(a)–15(c), does not show a clear behavior for all range of concentrations studied, making difficult to discern which mechanism of its criteria promotes negative wake formation. Nevertheless, the criterion is correct with negative wakes induced for values larger than the critical We number shown in Fig. 9.

Dou and Phan-Thien[21] and Bush[14] criteria show more explicitly that the extensional properties of the solution are the important factors for negative wake generation, in which a less strain-thickening extensional viscosity is closely related to the physical mechanism for its appearance. In this work, for the first time and in agreement with Dou and Phan-Thien criterion, it is clearly demonstrated that the shape of the extensional viscosity curve (i.e., the derivative of the extensional viscosity with the extension rate), the magnitude of the extension thickening peak and the onset for the extension thinning determine the critical We number for negative wake generation. Increasing wall effects accentuates the wake strength, as observed in Fig. 15(a).

A summary of Dou and Phan-Thien[21] criterion is de-

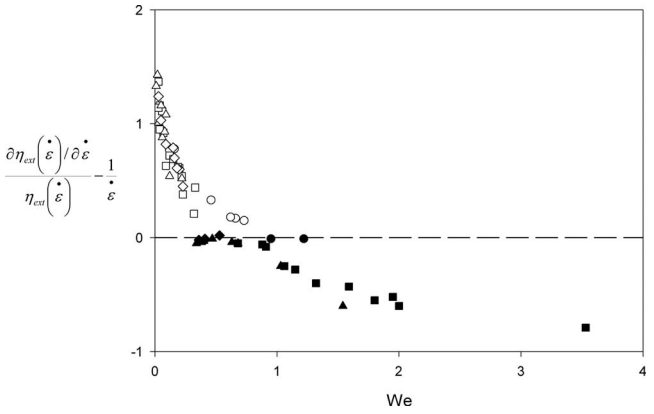

FIG. 16. Dou and Phan-Thien criterion for different fluids and different a/R: HASE 1.0% (circles), HASE 1.5% (squares), HASE 2.0% (triangles), and HASE 2.5% (diamonds).

picted in Fig. 16 where it is demonstrated that the aspect ratio, a/R, just accentuates the strength of the negative wake. Negative wakes appear when the two terms of the criterion become equal.

VI. CONCLUSIONS

The experimental and theoretical results shown in this work demonstrate that the extensional properties of the solutions and the characteristic extension rate are the most important factors for negative wake generation. The characteristic extension rate was defined as the sphere velocity divided by the distance from the rear of the sphere to the stagnant point where the flow reverses and forms the wake.

After evaluating the criteria proposed in literature for negative wake generation, the Dou and Phan-Thien[21] criterion reveals a plausible physical mechanism for generation of negative wakes. It considers that when the magnitude of the gradient of the extensional viscosity with respect to the extension rate divided by the extensional viscosity approaches the inverse of the extension rate as We increases, negative wakes can be generated. A lesser strain-thickening extension viscosity together with a high value of the reciprocal of the extensional rate will promote the formation of negative wakes.

The critical Weissenberg number for wake generation lies in the region around the peak of extension thickening near the onset for extension thinning. As We increases, the stagnant region where the flow reverses shifts closer to the sphere and the amplitude of the wake augments. Furthermore, increasing the wall proximity accentuates the strength of the wake and shifts the stagnant region closer to the sphere. The opposite occurs as inertia increases. Since the aspect ratio is not a key factor for wake generation, the negative wake may occur in unbounded flows.

In the case of Bush[14] and Harlen[18] criteria, it is also possible to determine a critical Weissenberg number. Nevertheless, a well-defined limit for generation of negative wake is not apparent, which means that neither the elasticity nor shear properties themselves can provide a physical mechanism for negative wake appearance. Conclusions reached by Dou and Phan-Thien[21] on the physical mechanisms for negative wake generation, are in agreement with the results exposed in this work.

ACKNOWLEDGMENTS

A.J.M.-F. acknowledges the support given by CONACYT. In addition, financing from project 47192 is gratefully acknowledged. The authors acknowledge the collaboration of F. Calderas, C. Palacios, and R. Ledesma in the rheological characterization and PIV technique implementation. We also wish to thank the reviewers for their helpful comments on the original version of this manuscript.

[1] B. Caswell, O. Manero, and B. Mena, "Recent developments on the slow viscoelastic flow past spheres and bubbles," Rheology Reviews, British Society of Rheology **2**, 197 (2004).
[2] G. H. McKinley, in *Transport Processes in Bubbles, Drops and Particles*, 2nd ed., edited by D. De Kee and R. P. Chhabra (Taylor & Francis, London, 2002).
[3] D. Sigli and M. Coutanceau, "Effect of finite boundaries on the slow laminar isothermal flow of a viscoelastic fluid around a spherical obstacle," J. Non-Newtonian Fluid Mech. **2**, 1 (1977).
[4] O. Hassager, "Negative wake behind bubbles in non-Newtonian liquids," Nature (London) **279**, 402 (1979).
[5] C. Bisgaard, "Velocity fields around spheres and bubbles investigated by laser-Doppler anemometry," J. Non-Newtonian Fluid Mech. **12**, 283 (1983).
[6] A. Maalouf and D. Sigli, "Effects of body shape and viscoelasticity on the slow flow around an obstacle," Rheol. Acta **23**, 497 (1984).
[7] M. D. Chilcott and J. M. Rallison, "Creeping flow of dilute polymer solutions past cylinders and spheres," J. Non-Newtonian Fluid Mech. **29**, 381 (1988).
[8] E. O. A. Carew and P. Townsend, "Non-Newtonian flow past a sphere in a long cylindrical tube," Rheol. Acta **27**, 125 (1988).
[9] R. Zheng, N. Phan-Thien, and R. I. Tanner, "On the flow past a sphere in a cylindrical tube: limiting Weissenberg number," J. Non-Newtonian Fluid Mech. **36**, 27 (1990).
[10] O. G. Harlen, "High Deborah number flow of a dilute polymer solutions past a sphere falling along the axis of a cylindrical tube," Rheol. Acta **37**, 157 (1990).
[11] B. Gervang, A. R. Davies, and T. N. Phillips, "On the simulation of viscoelastic flow past a sphere using spectral methods," J. Non-Newtonian Fluid Mech. **44**, 281 (1992).
[12] H. Jin, N. Phan-Thien, and R. I. Tanner, "A finite element analysis of the flow past a sphere in a cylindrical tube: PTT fluid model," Comput. Mech. **8**, 409 (1991).
[13] R. Zheng, N. Phan-Thien, and R. I. Tanner, "The flow past a sphere in a cylindrical tube: effects of inertia, shear-thinning and elasticity," Rheol. Acta **30**, 499 (1991).
[14] M. B. Bush, "On the stagnation flow behind a sphere in a shear-thinning viscoelastic liquid," J. Non-Newtonian Fluid Mech. **55**, 229 (1994).
[15] J. V. Satrape and M. J. Crochet, "Numerical simulation of the motion of a sphere in a Boger fluid," J. Non-Newtonian Fluid Mech. **55**, 91 (1994).
[16] O. G. Harlen, J. M. Rallison, and P. Szabo, "A split Lagrangian-Eulerian method for simulating transient viscoelastic flows," J. Non-Newtonian Fluid Mech. **60**, 81 (1995).
[17] P. Y. Huang and J. Feng, "Wall effects on the flow of viscoelastic fluids around a circular cylinder," J. Non-Newtonian Fluid Mech. **60**, 179 (1995).
[18] O. G. Harlen, "The negative wake generation behind a sphere sedimenting through a viscoelastic fluid," J. Non-Newtonian Fluid Mech. **108**, 411 (2002).
[19] M. T. Arigo and G. H. McKinley, "An experimental investigation of negative wakes behind spheres settling in a shear-thinning viscoelastic fluid," Rheol. Acta **37**, 307 (1998).
[20] H. S. Dou and N. Phan-Thien, "Negative wake in the uniform flow past a cylinder," Rheol. Acta **42**, 383 (2003).

[21] H. S. Dou and N. Phan-Thien, "Criteria of negative wake generation behind a cylinder," Rheol. Acta **43**, 203 (2004).
[22] F. Bautista, J. M. de Santos, J. E. Puig, and O. Manero, "Understanding thixotropic and antithixotropic behavior of viscoelastic micellar solutions and liquid crystalline dispersions. I. The model," J. Non-Newtonian Fluid Mech. **80**, 93 (1999).
[23] O. Manero, F. Bautista, J. F. A. Soltero, and J. E. Puig, "Dynamics of worm-like micelles: the Cox-Merz rule," J. Non-Newtonian Fluid Mech. **106**, 1 (2002).
[24] A. J. Mendoza-Fuentes, "Sedimentation study of particles in non-Newtonian fluids" Ph.D. thesis, National University of México, 2009.
[25] Y. Caram, F. Bautista, J. Puig, and O. Manero, "On the rheological modeling of associative polymers," Rheol. Acta **46**, 45 (2006).
[26] E. S. Boek, J. T. Padding, V. J. Anderson, P. M. J. Tardy, J. P. Crawshaw, and J. R. A. Pearson, "Constitutive equations for extensional flow of wormlike micelles: stability analysis of the Bautista-Manero model," J. Non-Newtonian Fluid Mech. **126**, 39 (2005).
[27] H. Tan, K. C. Tam, V. Tirtaatmadja, R. D. Jenkins, and D. R. Bassett, "Extensional properties of model hydrophobically modified alcali-soluble associative (HASE) polymer solutions," J. Non-Newtonian Fluid Mech. **92**, 167 (2000).